ARTICLE IN PRESS

GSF-101141; No of Pages 10

Geoscience Frontiers xxx (2021) xxx



Contents lists available at ScienceDirect

Geoscience Frontiers

journal homepage: www.elsevier.com/locate/gsf



Research Paper

Quantifying the response of surface urban heat island to urbanization using the annual temperature cycle model

Huidong Li ^a, Yuyu Zhou ^{a,*}, Gensuo Jia ^b, Kaiguang Zhao ^c, Jinwei Dong ^d

- ^a Department of Geological and Atmospheric Sciences, Iowa State University, Ames 50011, USA
- b Key Laboratory of Regional Climate-Environment for Temperate East Asia, Institute of Atmospheric Physics, Chinese Academy of Sciences, Beijing 100029, China
- ^c Ohio Agricultural Research and Development Center, School of Environment and Natural Resources, The Ohio State University, Wooster, OH 44691, USA
- d Key Laboratory of Land Surface Pattern and Simulation, Institute of Geographic Sciences and Natural Resources Research, Chinese Academy of Sciences, Beijing 100101, China

ARTICLE INFO

Article history: Received 13 September 2020 Received in revised form 18 December 2020 Accepted 28 December 2020 Available online xxxx

Keywords: Urban heat island Urbanization Spatiotemporal dynamics Annual temperature cycle model Diurnal temperature range

ABSTRACT

Urban heat island (UHI), driving by urbanization, plays an important role in urban sustainability under climate change. However, the quantification of UHI's response to urbanization is still challenging due to the lack of robust and continuous temperature and urbanization datasets and reliable quantification methods. This study proposed a framework to quantify the response of surface UHI (SUHI) to urban expansion using the annual temperate cycle model. We built a continuous annual SUHI series at the buffer level from 2003 to 2018 in the Jing-Jin-Ji region of China using MODIS land surface temperature and imperviousness derived from Landsat. We then investigated the spatiotemporal dynamic of SUHI under urban expansion and examined the underlying mechanism. Spatially, the largest SUHI interannual variations occurred in suburban areas compared to the urban center and rural areas. Temporally, the increase in SUHI under urban expansion was more significant in daytime compare to nighttime. We found that the seasonal variation of SUHI was largely affected by the seasonal variations of vegetation in rural areas and the interannual variation was mainly attributed to urban expansion in urban areas. Additionally, urban greening led to the decrease in summer daytime SHUI in central urban areas. These findings deepen the understanding of the long-term spatiotemporal dynamic of UHI and the quantitative relationship between UHI and urban expansion, providing a scientific basis for prediction and mitigation of UHI.

© 2021 China University of Geosciences (Beijing) and Peking University. Production and hosting by Elsevier B.V. This is an open access article under the CC BY license (http://creativecommons.org/licenses/by/4.0/).

1. Introduction

Urbanization alters surface energy budget, resulting in higher temperatures in urban areas than in surrounding rural areas, which is called urban heat island (UHI) effect. Air temperatures in the central areas of big cities can be more than 10 K higher than that in the neighboring rural areas (Oke, 1982). Elevated temperatures strengthen heat waves in summer (Constantinescu et al., 2016), especially under the background of climate change. Compared to rural residents, urban residents usually suffer more from heat stress, directly threatening their health (Wang et al., 2019). Moreover, higher temperatures increase the consumptions of building energy (Li et al., 2019c) and urban water (Guhathakurta and Gober, 2007) in summer and affect the urban vegetation (Alberti et al., 2017; Li et al., 2017a; Meng et al., 2020) and air pollution (Li et al., 2018a, 2020). UHI has become an important factor of urban sustainability because of continuous urbanization and climate change (Wu, 2014). Quantifying the spatiotemporal dynamic

* Corresponding author. E-mail address: yuyuzhou@iastate.edu (Y. Zhou). of UHI and its response to urbanization is necessary to better identify and assess the possible heat risk in cities.

Although UHI has been investigated over the decades, the spatiotemporal dynamic of UHI at a large scale has only been revealed during the satellite era. Remote sensing provides observations for monitoring surface UHI (SUHI) at the city, regional, and even global scales. At a city scale, SUHI spatial pattern and driving factors have been widely investigated by analyzing the relationships between SUHI and various landscape indexes (Tang et al., 2017; Yue et al., 2019; Liu et al., 2020). For example, Connors et al. (2013) assessed the relationship between landscape configuration and SUHI and modeled the determinants of SUHI in Phoenix using ASTER data. Li et al. (2018b) investigated the relationship between SUHI and imperviousness and developed a new method for the quantification of SUHI intensity in Berlin using MODIS data. At the regional and global scales, the spatial variations of SUHI across cities were analyzed. For example, Zhou et al. (2017) and Li et al. (2017b) revealed the relationship between SUHI and city size and population in Europe and North America using MODIS data. Peng et al. (2012) and Chakraborty and Lee (2019) investigated the global SUHI characteristics and revealed the dominant driving factors behind using MODIS data.

https://doi.org/10.1016/j.gsf.2021.101141

1674-9871/© 2021 China University of Geosciences (Beijing) and Peking University. Production and hosting by Elsevier B.V. This is an open access article under the CC BY license (http://creativecommons.org/licenses/by/4.0/).

Please cite this article as: H. Li, Y. Zhou, G. Jia, et al., Quantifying the response of surface urban heat island to urbanization using the annual temperature c..., Geoscience Frontiers, https://doi.org/10.1016/j.gsf.2021.101141

However, most previous studies mainly explored SUHI's spatial pattern in short periods (i.e., daily and seasonal). Analysis of long-term spatiotemporal dynamic of SUHI remains a challenge, due to the limitations in the acquisition of long-term and continuous remote sensing land surface temperature (LST) data (Zhou et al., 2019). With the extended and continuous remote sensing observations over time, the investigation of the interannual SUHI dynamic using satellite data has become possible. For example, Yao et al. (2019) investigated the long-term variation of SUHI globally using MODIS data and revealed the influence of rural greening on SUHI. Even though, the data continuity is still a major challenge in studying long-term SUHI using remote sensing data (Zhou et al., 2019). This is because remote sensing LST data usually have a large number of missing pixels, due to the disturbance of cloud contaminations. Especially in urban areas, the spatial coverage of valid pixels of remote sensing LST is intrinsically lower than that in rural areas (Hu and Brunsell, 2013). Li et al. (2018c) reported that the available MODIS daily LST cover is less than one-third for urban areas in the conterminous United States. To overcome this problem, some gap filling methods, such as time aggregation and spatiotemporal interpolation, have been developed. However, the time aggregation method decreases the temporal resolution and spatiotemporal interpolation method usually costs a larger number of computing resources (Li et al., 2018c). A more efficient approach is needed to generate a continuous LST time series for the long-term SUHI study.

The Annual Temperature Cycle (ATC) model offers an alternative approach to generate a continuous temperature series on the annual time scale (Bechtel, 2012). The ATC model fits the annual LST cycle, which shows a comparable deterministic variation in the irradiation, as a single sinusoidal function. The derived LST represents the climatology of annual LST on an annual time scale. The robustness of the ATC model has been widely validated using both MODIS (Bechtel, 2015; Zou et al., 2018) and Landsat datasets (Bechtel, 2012; Weng and Fu, 2014). Moreover, the ATC model can be used to generate continuous LST data at a large spatial scale. For example, Bechtel (2015) generated a global LST dataset using the ATC model and MODIS data. Because of the above advantages, the ATC model has been successfully used to study SUHI in various regions. For example, Huang et al. (2016) validated the reliability of the ATC model in quantifying SUHI intensity in Beijing and Shanghai. Bechtel et al. (2019) compared the SUHI of 50 cities across the globe from the ATC model and established a consistent and comprehensive SUHI analysis framework. However, few studies employed the ATC model to investigate the interannual dynamic of SUHI (Weng and Fu, 2014). Moreover, the derived overall SUHI intensity based on the urban-rural dichotomy approach in previous studies (Bechtel, 2015; Huang et al., 2016) cannot reflect the spatial variation of SUHI. Some studies proposed to divide a city into several buffers and calculate SUHI intensity in each buffer (Hu and Brunsell, 2015; Li et al., 2018b). The mean SUHI in each buffer represents the overall thermal characteristic of the buffer. The ATC model can be used at the buffer level to reduce computing time.

This study proposed a framework to quantify the response of SUHI to urban expansion at buffer level in the Beijing-Tianjin-Hebei (Jing-Jin-Ji (III)) region using the ATC model. We first estimated buffer specific parameters in the ATC model using MODIS land surface temperature and imperviousness derived from a high-resolution urban map and developed an annual SUHI time series from 2003 to 2018 at the buffer level in 13 major city clusters in the JJJ region. Then we investigated the relationship between ATC model parameters and imperviousness and the spatiotemporal dynamic of SUHI across urban-rural gradients. Finally, we examined and discussed the underlying mechanism of SUHI's spatiotemporal dynamic. The derived SUHI time series from the ATC model can contribute a deeper understanding of the long-term and continuous spatiotemporal dynamic of UHI, and the relationship between the ATC model parameters and imperviousness reveals the quantitative response of UHI to urban expansion, providing a scientific basis for prediction and mitigation of future heat stress.

2. Study area, data and methodology

2.1. Study area

The study area is the JJJ region of China (Fig. 1a). The JJJ region is located at North China Plain and occupies ~218,000 km² area. The population in this region is ~111 million in 2014, accounting for more than 8% of the national population in China. There are a total of 13 prefecture and higher-level city clusters in this region, including three large cities (i.e., Beijing, Tianjin, and Shijiazhuang). The JJJ region is recognized as one of China's most dynamic urban cluster with fast urban expansion in the past several decades, which significantly alters the local urban climate. Therefore, the JJJ region serves as an ideal area for UHI study.

2.2. Data

The major remote sensing datasets, including LST, impervious surface areas (ISA), and urban cluster map, were used. LST data was used to calculate the SUHI, which was then used to estimate the ATC model parameters. The urban cluster map was used to determine the boundary of each city. The ISA was used to build buffers and quantify urban expansion.

MODIS daily LST product collection 6 at a resolution of 1 km was used. MODIS LST product was retrieved by the generalized splitwindow algorithm. The retrieved LST was further refined by correcting the biases. The collection 6 dataset has high accuracy with errors within ± 1 K in most cases (Wan, 2014). MODIS LST has been widely applied to study SUHI regionally (Li et al., 2017b) and globally (Chakraborty and Lee, 2019). This study used the MODIS LST product (MYD11A1) from Aqua satellite with overpass time of $\sim 01:30$ pm (approximating daily maximum) and $\sim 01:30$ am (approximating daily minimum). In addition, MODIS monthly Enhanced Vegetation Index (EVI) product (MOD13A3) at a resolution of 1 km was used to investigate the variation of vegetation. MODIS water product (MOD44W) at a resolution of 500 m was also used to exclude the water pixels in calculating SUHI intensity.

Percent ISA was calculated from an urban map at a resolution of 30 m. The urban map from 2003 to 2015 was from Li et al. (2018e) using annual Landsat time series data and a temporal segmentation approach. We calculated the percent ISA value by aggregating the 30 m urban map data to the spatial resolution of MODIS LST data. Urban cluster map was developed by Zhou et al. (2014, 2015a, 2015b, 2018) using nighttime light data based on a cluster-based method. This urban cluster map can accurately capture the boundary of cities globally and has been successfully used to study UHI (Li et al., 2017b). The most recent urban cluster map in 2013 was used.

2.3. Methodology

This study developed a framework to quantify spatiotemporal dynamics of SUHI and its response to urbanization using the ATC Model. The framework includes three key steps: (1) quantifying SUHI intensity at the buffer level, (2) fitting the annual cycle of SUHI using the ATC model, and (3) analyzing the response of SUHI to urbanization.

2.3.1. Quantifying SUHI intensity

We quantified SUHI intensity at the buffer level using MODIS data. First, we built buffers in the areas of the urban cluster and the surrounding rural zone (Fig. 1b). The boundary of each city cluster were determined using the urban cluster map. The surrounding rural zone was defined as the areas within the ring zone around the urban cluster, which was three times of the urban cluster areas based on the study of Zhou et al. (2015a). The buffers were built based on ISA data. Given the footprint effect of LST observation, we used the Kernel Density Estimation (KDE) method to regionalize ISA, referring to the study of Li et al. (2018b). The KDE calculation was conducted with a search radius of

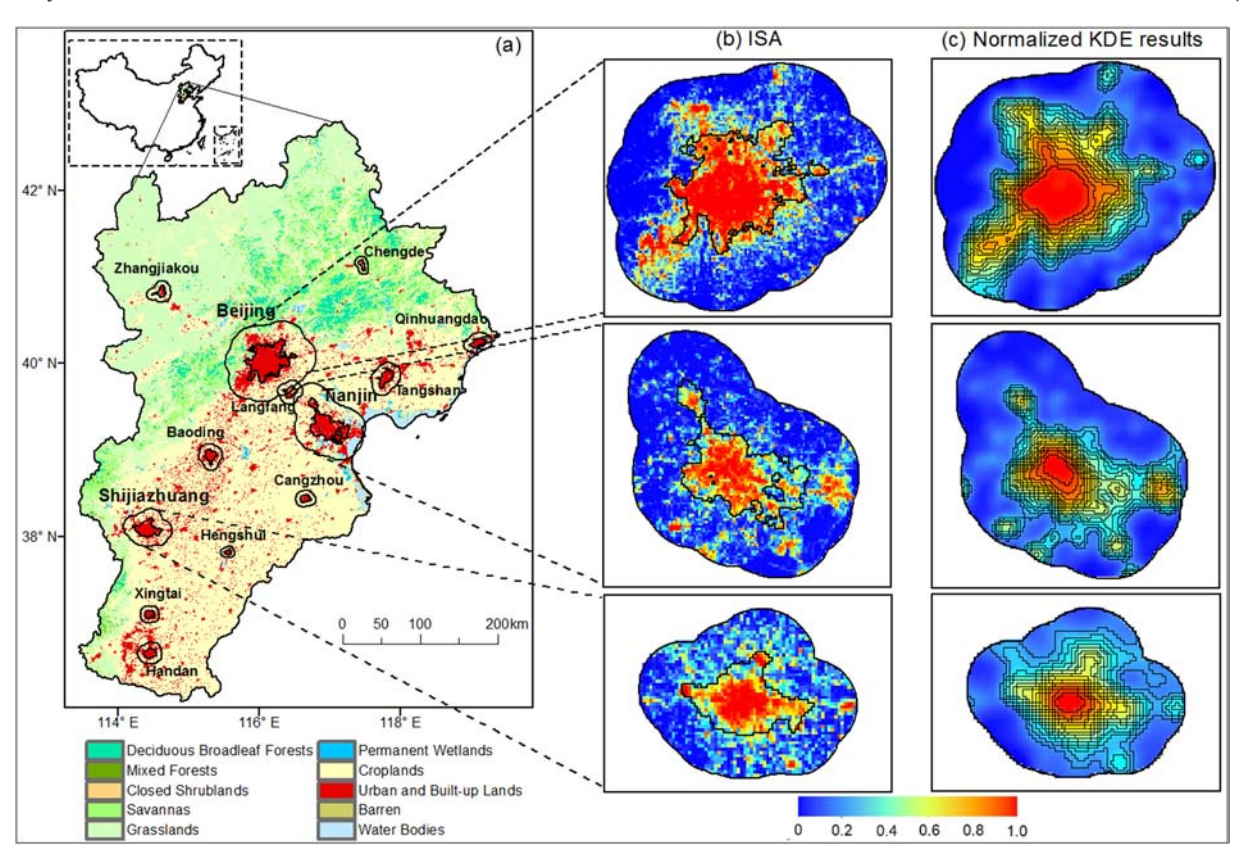


Fig. 1. (a) The location and land-cover/land-use map of the JJJ region, and spatial patterns of (b) Impervious Surface Area (ISA), and (c) normalized kernel density estimation (KDE) and buffers in Beijing, Tianjin, and Shijiazhuang, China. The black lines surrounding the cities in (a) indicate the boundaries of urban clusters and its surrounding rural zones. The black lines in (c) indicate the buffers boundaries. The backgrounds in (b) and (c) show the ISA in 2015 and the derived buffers.

10 km using the sp.kde function of library spatialEco (https://cran.rproject.org/web/packages/spatialEco/index.html) on R3.4.3. The KDE calculation results were further normalized to 0 to 1 (Fig. 1c). Based on the normalized KDE results, each city was divided into 20 buffers with a constant interval of 0.05. Then the LST difference between buffers and the background buffer close to the rural zone was calculated as the SUHI intensity. The background buffer was the reference for SUHI intensity calculation. To reduce the uncertainty of derived SUHI intensity, we combined the first four buffers close to the rural zone frontier as the background buffer. Each city, therefore, has 17 buffers with numbers ranging from 1 (outside) to 17 (inside), and the SUHI in the reference buffer was 0. To decrease the uncertainties in the derived SUHI, the raw LST data with the coverage of valid pixels lower than 1/3 in the urban cluster or the total areas of the urban cluster and rural zone were excluded during the calculation. In addition, the pixels with water and high elevation (100 m higher than the mean elevation of urban pixels) were excluded from the calculation of SUHI.

2.3.2. Fitting the annual cycle of SUHI

We fitted the annual cycle of SUHI in each buffer using the ATC model. The parameters in the ATC model were estimated using the quantified SUHI in the first step. The ATC model fits the annual LST cycle as a single sinusoidal function (Bechtel, 2012). The annual SUHI cycle is the difference of the annual LST cycles in urban and rural areas and also can be fitted using a single sinusoidal function (Huang et al., 2016). The function of annual SUHI cycle was expressed as:

$$SUHI(DOY) = S_M + S_A \times \sin(2\pi \cdot DOY/365 + S_P)$$
 (1)

where S_M , S_A , and S_P represent the mean, amplitude, and the phase shift of the annual SUHI cycle. To better understand the physical meaning of

 S_P , it is converted to S_P = $-2\pi \cdot S_{P_DOY}/365 + \pi/2$, where S_{P_DOY} represents the DOY when the annual SUHI cycle reaches its maximum. Huang et al. (2017) found that the S_{P_DOY} has rather minor urbanrural variations. In this study, we set S_{P_DOY} a constant parameter in each city and calculated its value using the observed SUHI data in all the buffers from MODIS data. Then we calculated the values of S_M and S_M in each buffer based on the observed SUHI in the buffer. The parameters in Eq. (1) was calculated using the nlsLM function of library minpack.lm (https://cran.r-project.org/web/packages/minpack.lm/index.html) in R3.4.3. We fitted the annual SUHI cycle in each buffer from 2003 to 2018. The derived dynamic of SUHI was evaluated against the observed SUHI using two indicators, the correlation coefficient (r) and mean absolute error (MAE).

2.3.3. Analyzing the response of SUHI to urban expansion

We analyzed the response of SUHI to urbanization in two ways. First, we extracted the estimated ATC model parameters (S_M and S_A) and investigated their relationship with the urbanization indicator, ISA, across the urban-rural gradient, given that these two parameters reflect the mean and amplitude of the annual SUHI cycle. Second, we investigated the spatiotemporal dynamic of the annual SUHI cycle, including the interannual variations of the spatial patterns of SUHI in different seasons and the spatial variations of annual SUHI cycle across the urban-rural gradient. To better capture of the interannual trend of SUHI under urbanization, we calculated the moving average of annual SUHI cycle over five years, when investigating its interannual dynamic. In addition, to explore the mechanism behind the spatiotemporal variation of SUHI, we calculated the diurnal temperature range (DTR), the difference of daytime and nighttime LST, at each buffer and its difference with that at the background buffer ($\Delta_{\text{u-r}}$ DTR).

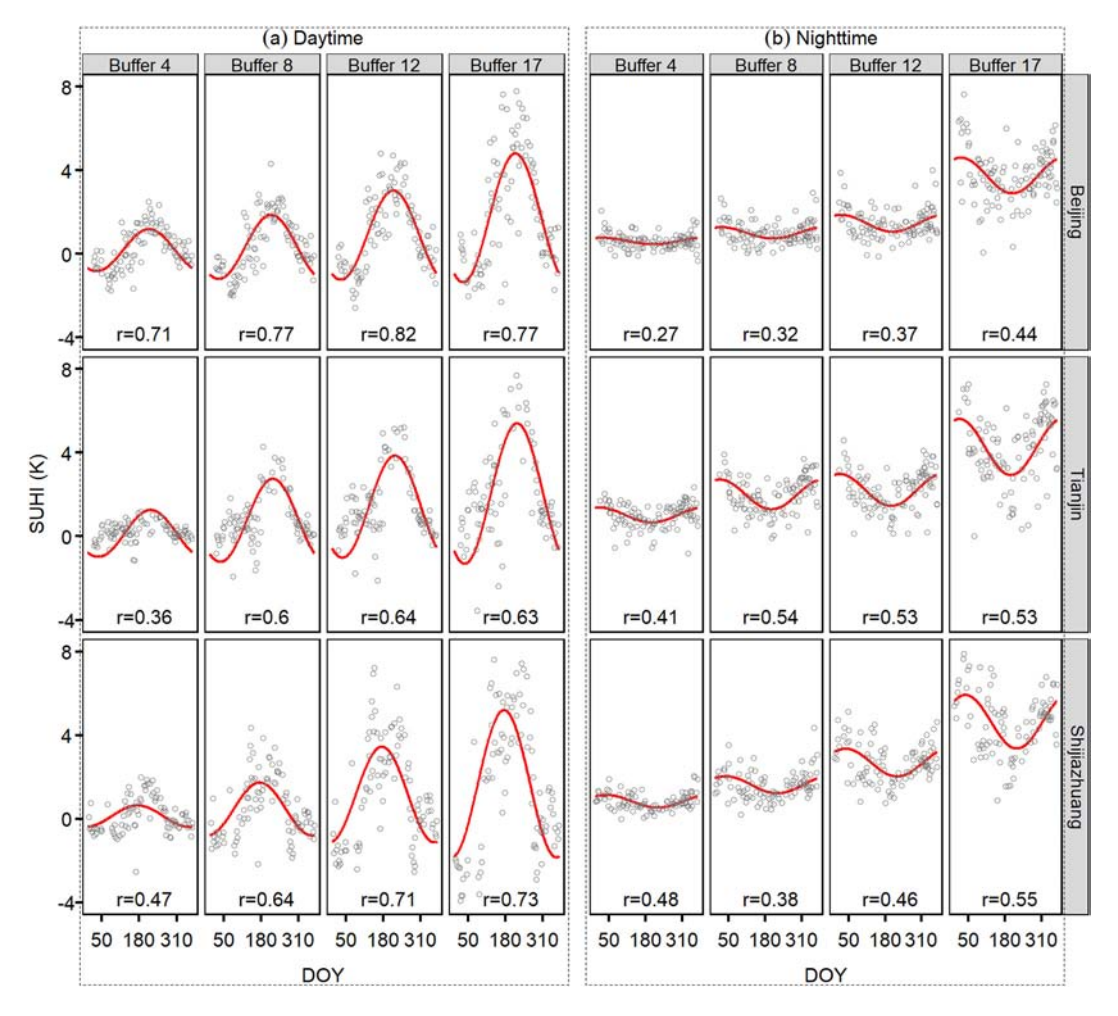


Fig. 2. Comparison of annual SUHI cycles derived from the ATC model (red line) and observations (dots) in the (a) daytime and (b) nighttime in four selected buffers in 2010 in Beijing, Tianjin, and Shijiazhuang, China.

3. Results

3.1. The performance of the ATC model

Generally, the derived annual SUHI cycle from the ATC model agreed with observations. Both of them showed the maximum values in summer daytime and winter nighttime (Fig. 2). The derived SUHI in the buffers close to urban center showed higher correlations with observations than that in the buffers close to rural areas. The overall averaged MAE of derived daily SUHI during the study period was 0.57 K for Beijing, which is slightly larger than that 0.3 K in the study of Huang et al. (2016). The reason for the larger bias in this study was that we calculated the spatial variation of SUHI at different buffers, while Huang only calculated the mean SUHI intensity in the urban cluster. Among all 13 cities in the JJJ region, the overall MAE of daily SUHI ranged from 0.48 to 0.86 K (Table 1). Daytime SUHI had a larger bias than nighttime SUHI.

3.2. Spatial patterns of ATC parameters

The ATC model parameters, S_M and S_A , showed significant urbanrural variations (Fig. 3). Both of them decreased from urban center to rural areas, indicating the higher mean and amplitude of annual SUHI cycle in the urban center. The spatial differences of S_M were up to 1.7-2.3~K and 4.1-4.8~K in the daytime and nighttime, respectively, and the spatial differences of S_A were up to 3.3-3.5~K and 1.2-1.4~K. The diurnal variations of S_M and S_A were opposite. S_M was higher at night, while S_A was higher in the day, indicating the larger annual mean SUHI at night and larger annual amplitude of SUHI during the day. The reason of the larger annual mean SUHI at night is that the nighttime SUHI was always positive, while the daytime SUHI was only positive in summer, but negative in winter (Fig. 2). The larger annual amplitude of daytime SUHI is related to the larger seasonal variation of solar radiation, the major driving factor of daytime SUHI, compared to that of stored heat, the major driving factor of nighttime SUHI. Both

Table 1
The mean absolute error (MAE) between derived and observed SUHI from 2003 to 2018 in 13 cities in the ||| region.

City	BJ	TJ	SJZ	BD	CZ	TS	HD	HS	LF	QHD	XT	CD	ZJK
Daily	0.57	0.72	0.86	0.66	0.73	0.68	0.69	0.73	0.62	0.79	0.70	0.48	0.76
Day	0.69	0.89	1.17	0.89	0.92	0.82	0.88	0.89	0.73	1.10	0.95	0.66	1.04
Night	0.48	0.58	0.59	0.49	0.59	0.55	0.52	0.60	0.52	0.54	0.48	0.30	0.53

Note: BJ, Bejing; TJ, Tianjin; SJZ, Shijiazhuang; BD, Baoding; CZ, Cangzhou; TS, Tangshan; HD, Handan; HS, Hengshui; LF, Langfang; QHD, Qinhuangdao; XT, Xingtai; CD, Chengde; ZJK, Zhangiakou.

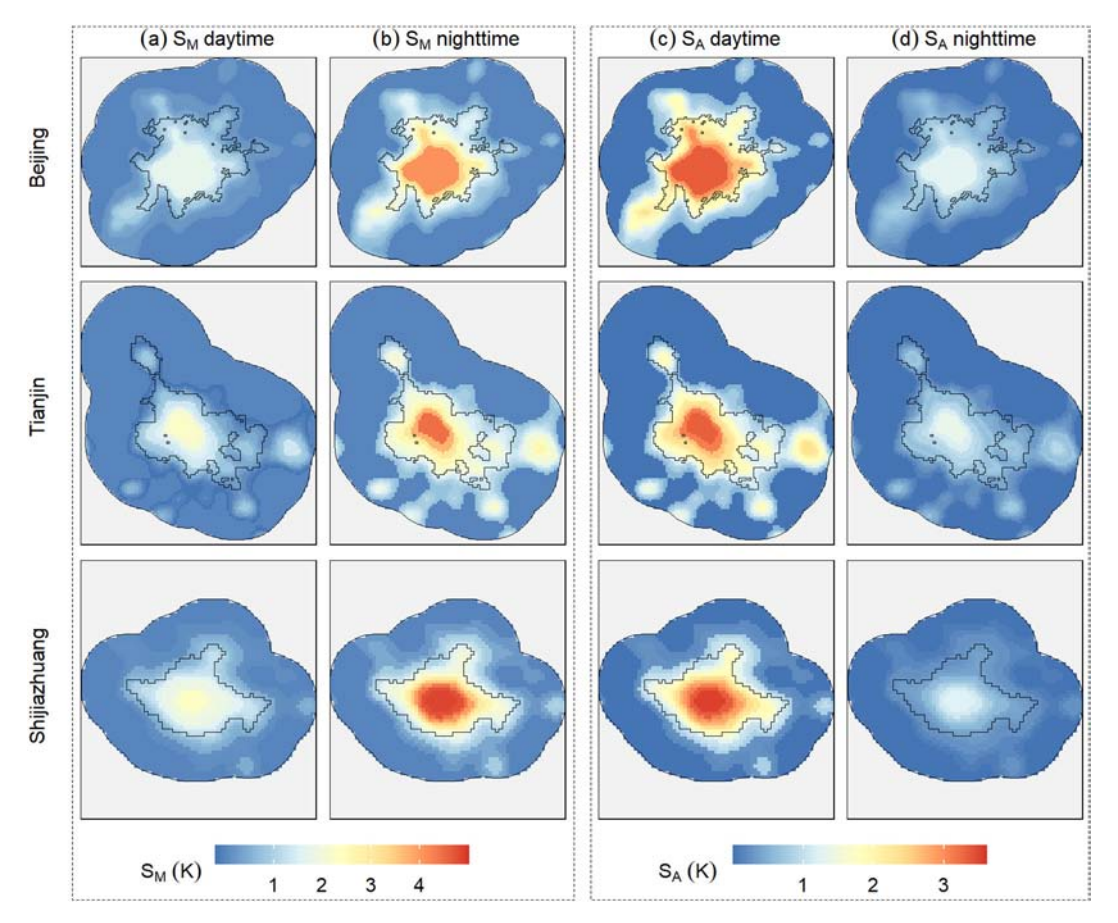


Fig. 3. Spatial patterns of ATC model parameters (a,b) S_M and (c,d) S_A in Beijing, Tianjin, and Shijiazhuang, China. The values here are the mean during 2003–2018.

the mean S_M and S_A during 2003–2015 were closely correlated with ISA over urban-rural gradients (Fig. 4). In Beijing, the correlation coefficients between S_M and S_A and ISA were 0.91 and 0.91 for daytime and

0.92 and 0.91 for nighttime, respectively. Both S_M and S_A showed increasing trends with the increase in ISA, indicating that urbanization is an important influencing factor of annual SUHI cycle.

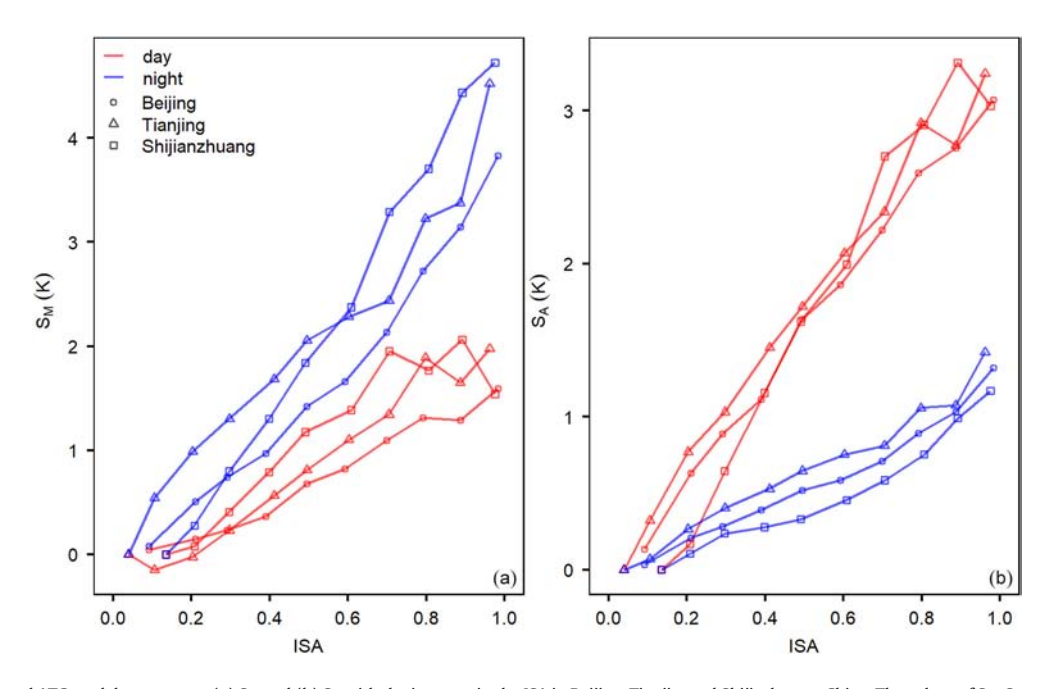


Fig. 4. Variations of annual ATC model parameters (a) S_M and (b) S_A with the increase in the ISA in Beijing, Tianjin, and Shijiazhuang, China. The values of S_M , S_A , and ISA in each buffer are the average during 2003–2015.

3.3. Dynamics of SUHI patterns

The SUHI showed remarkable temporal (i.e., annual, seasonal, and diurnal) variations (Fig. 5, Supplementary Figs. A.1 and A.2). In spring, summer, and autumn, the daytime SUHI was positive, with the highest intensity of 1.1, 5.0, and 2.8 K in the urban center of Beijing during the study period. The interannual variations of daytime SUHI in these seasons presented increasing trends in suburban buffers, but decreasing trends in urban center. Daytime SUHI became negative in winter, with the lowest density of $-1.5~\rm K$ in the urban center of Beijing. Moreover, the interannual variation of SUHI spatial pattern in winter daytime presented decreasing trends from 2003 to 2018. On the contrary, nighttime

SUHI was always positive, with the highest intensity of 5.7 K in winter. The interannual variation of nighttime SUHI presented slightly increasing trends from 2003 to 2018 in both suburban and urban buffers, especially in winter.

3.4. Dynamics of annual SUHI cycle

The interannual variations of annual SUHI cycle varied among the buffers (Fig. 6). Generally, the annual SUHI cycles in the suburban buffers showed larger interannual variations than those in the buffers close to the urban center and rural areas. This is mainly because the suburban areas experienced more significant urbanization process,

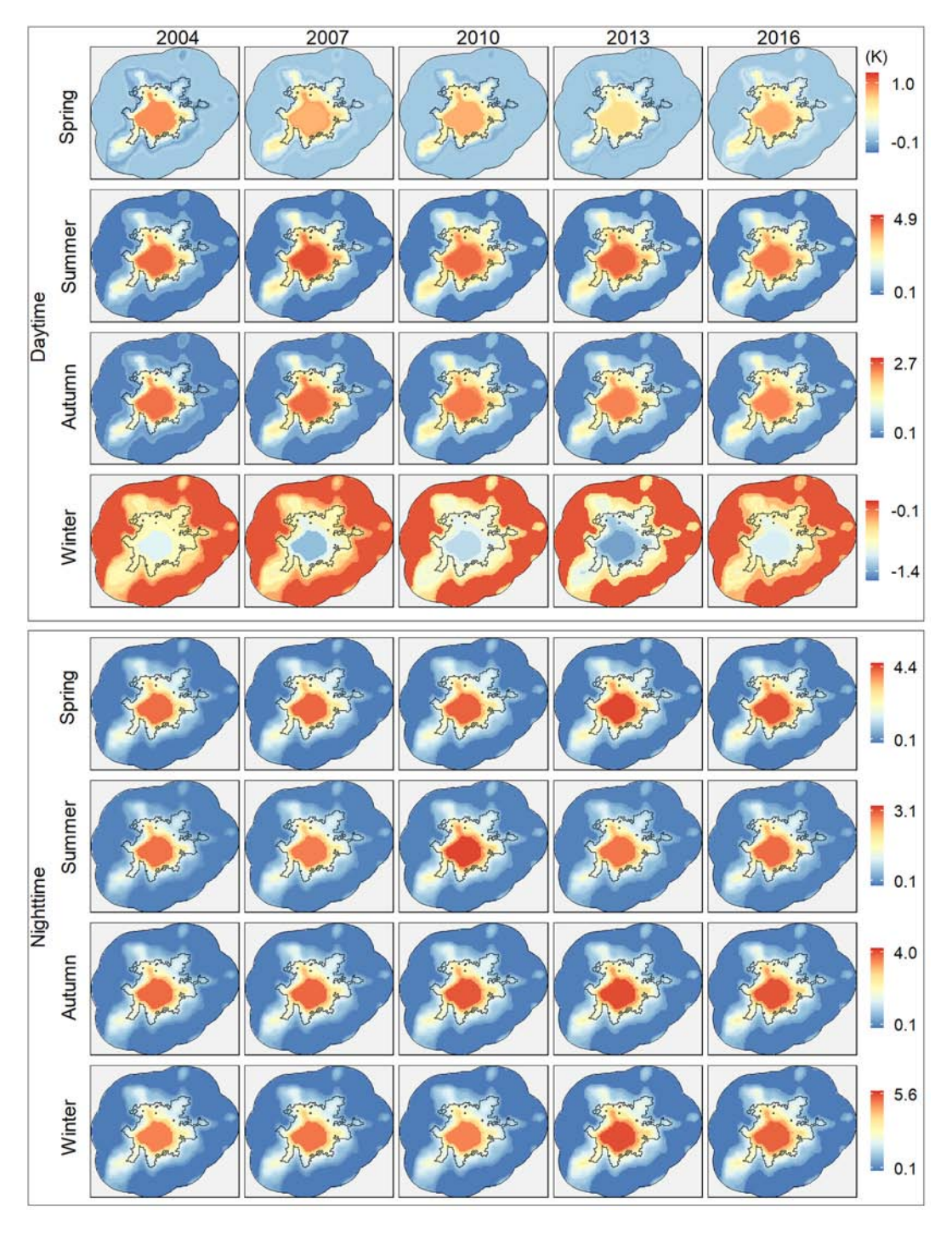


Fig. 5. Spatiotemporal patterns of derived SUHI in the winter, spring, summer, and autumn in Beijing. Winter: December, January, and February; Spring: March, April, and May; Summer: June, July, and August; Autumn: September, October, and November.

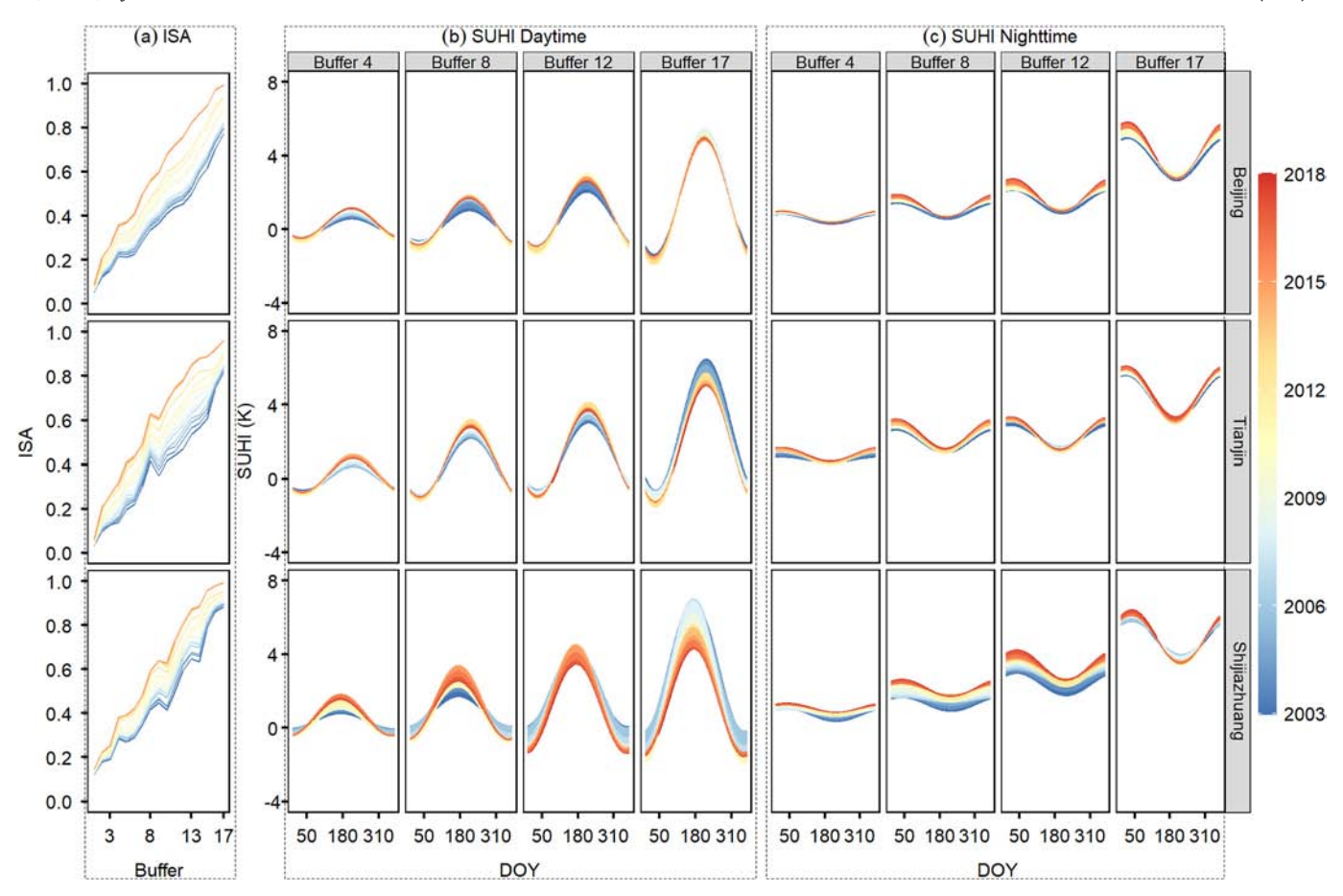


Fig. 6. Interannual dynamics of (a) ISA and derived annual SUHI cycle in the (b) daytime and (c) nighttime in four selected buffers in Beijing, Tianjin, and Shijiazhuang from 2003 to 2018. The annual SUHI cycles in this figure are the moving average of five years.

with larger interannual increases of ISA than the buffers in the central and rural areas (Fig. 6a). Moreover, daytime SUHI showed larger interannual variations of annual SUHI cycles than nighttime SUHI, indicating a higher sensitivity of daytime SUHI to urbanization. In addition, the interannual variation of summer daytime SUHI in the central buffer areas showed decreasing trends in all the three cities, in spite of the increase in ISA in these buffers. The reasons will be discussed in the Section 4. On the contrary, the nighttime SUHI did not show similar interannual trends with the daytime SUHI in the urban center.

3.5. Spatiotemporal dynamics of DTR

The urban-rural difference of diurnal temperature range ($\Delta_{\text{u-r}}DTR$) showed significant spatiotemporal variations (Fig. 7, Supplementary Fig. A.3). Generally, the $\Delta_{\text{u-r}}DTR$ decreased from rural areas to urban center, with negative values in winter, spring, and autumn, while it increased from the rural areas to urban center, with positive values in summer. The seasonal variation of $\Delta_{\text{u-r}}DTR$ indicated a lower daytime SUHI than nighttime SUHI in most of the days in a year, except for summer days. The interannual dynamic of $\Delta_{\text{u-r}}DTR$ showed increasing

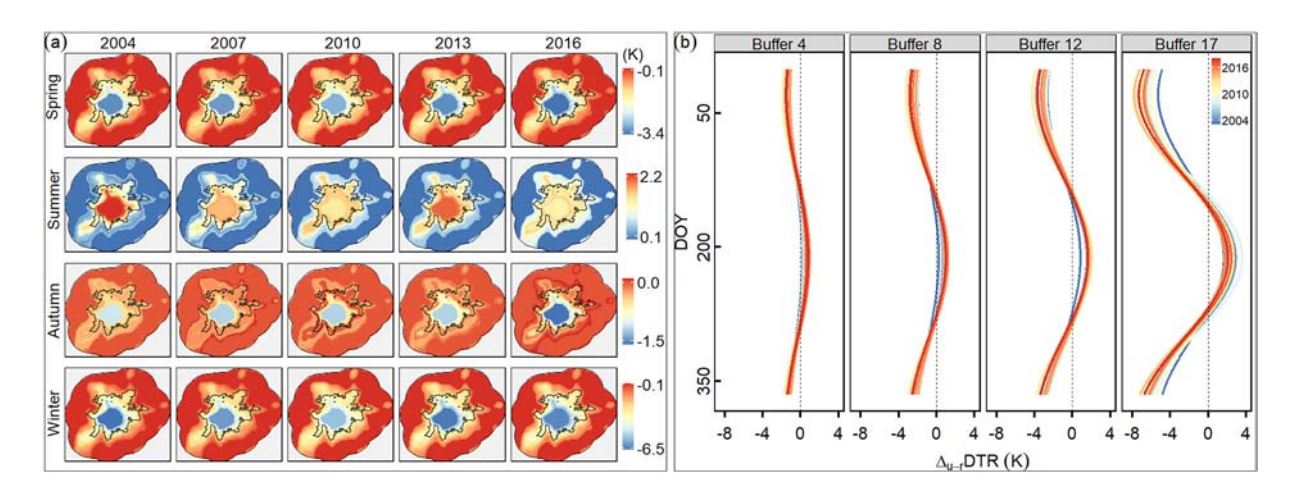


Fig. 7. Interannual dynamics of (a) spatial and (b) temporal patterns of DTR urban-rural difference derived from the ATC model in Beijing from 2003 to 2018. The annual Δ_{u-r} DTR cycles in this figure are the moving average of five years.

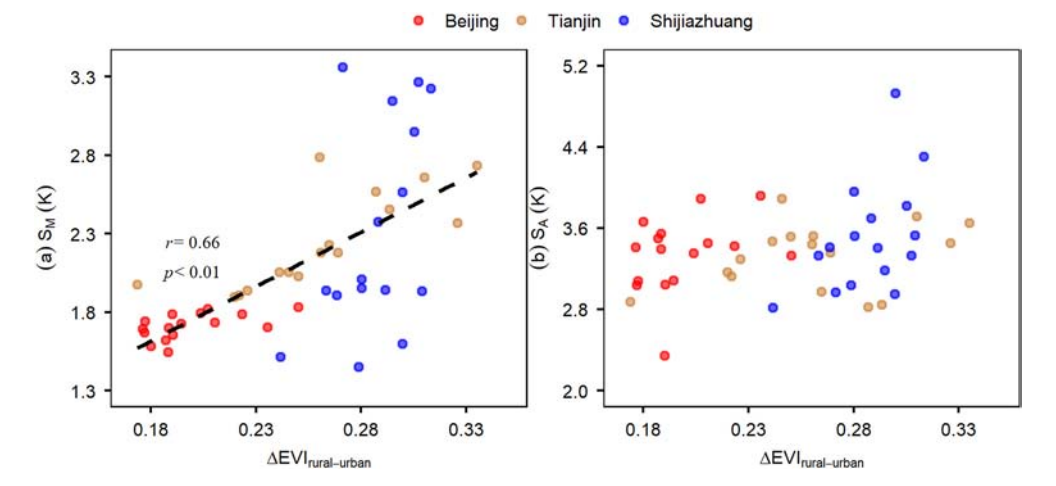


Fig. 8. The relationship between the daytime ATC model parameters (a) S_M and (b) S_A with the rural-urban difference of EVI. The rural buffer refers to the first four buffers close to the rural zone frontier, and the urban buffer refers to the innermost buffer in the urban center. Both the model parameters and EVI in this figure are the moving averages of five years.

trends in summer, but decreasing trends in winter. That means the daynight difference of SUHI became larger in both winter and summer. Additionally, the seasonal variation of $\Delta_{\text{u-r}}\text{DTR}$ was more significant in urban center buffers with large ISA, while its interannual variation was more significant in suburban areas, where the ISA showed a larger interannual increase.

4. Discussion

SUHI is mainly influenced by the urban-rural differences in the surface energy budget and the sensitivity of the surface to the absorbed heat (Varquez and Kanda, 2018). The energy balance basis of SUHI has been widely investigated (Oke, 1982; Christen and Vogt, 2004; Li

et al., 2019a) and in the study areas (Wang et al., 2007). To further understand the mechanism of SUHI in the JJJ region, we examined the surface's sensitivity to absorbed heat through the discussion of DTR because DTR has a negative relationship with surface thermal inertia (Carnahan and Larson, 1990).

In the JJJ regions, the negative Δ_{u-r} DTR in winter indicated the larger thermal inertia in rural areas, while the positive Δ_{u-r} DTR in summer indicated the larger thermal inertia in urban areas (Fig. 7). The seasonal variation of the urban-rural difference in the thermal inertia was mainly controlled by the rural areas, which is covered by the vegetation (crops & grassland, Fig. 1a) in the growing season, but becomes bare land in the non-growing season. Among urban, vegetation, and bare land, vegetation has the lowest thermal inertia, while bare land has the highest

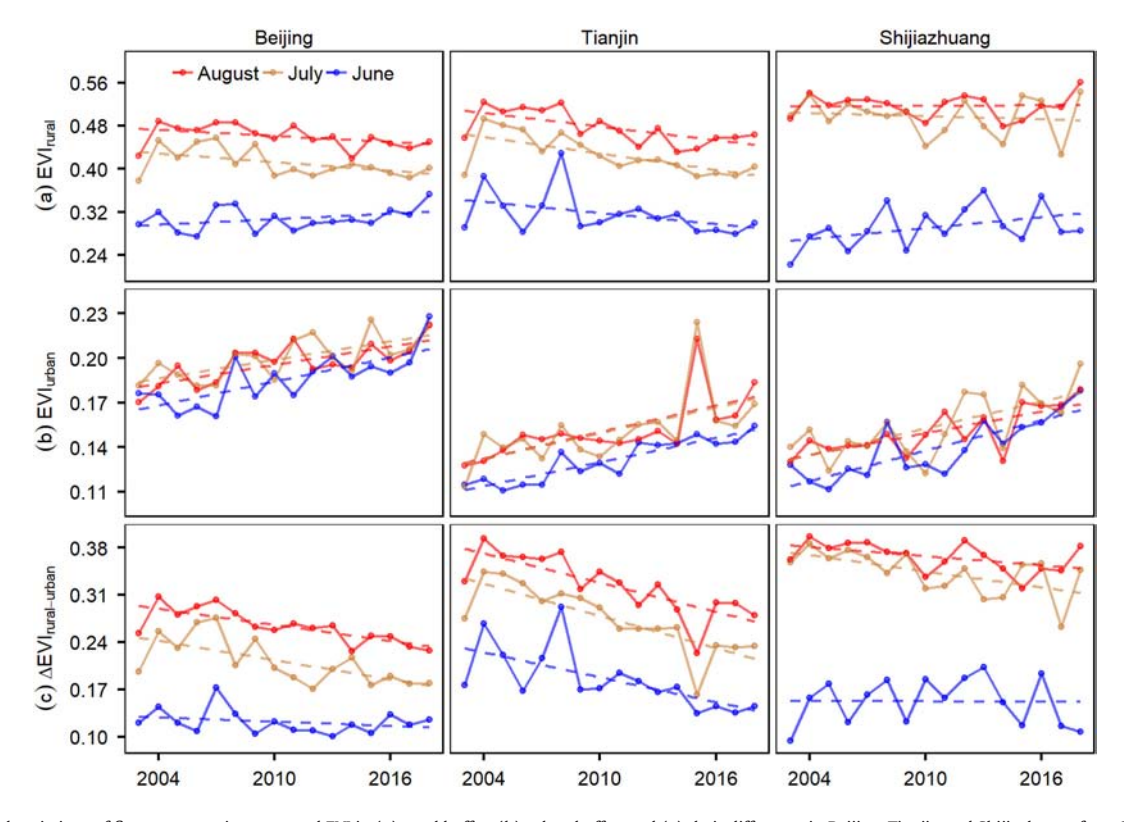


Fig. 9. Interannual variations of five years moving averaged EVI in (a) rural buffer, (b) urban buffer, and (c) their difference in Beijing, Tianjin and Shijiazhuang from 2003 to 2018. The buffers and moving average are same as those in Fig. 8.

one (Wang et al., 2007). In the non-growing season, the urban-rural difference in the energy balance was small and the urban-rural difference in the thermal inertia dominated SUHI. Due to the lower thermal inertia in rural areas, its surface was heated faster in the daytime and cooled faster at night, leading to a small and even negative daytime SUHI and a large and positive nighttime SUHI. However, in the growing season, vegetation covering in the rural areas could significantly increase the urban-rural difference of evapotranspiration during the day, leading to large daytime SUHI (Li et al., 2016, 2018d; Zhao et al., 2019). Meanwhile, larger thermal inertia in urban surface fastened surface heating during the day and surface cooling at night, further contributing to the increase in daytime SUHI and leading to the decrease in nighttime SUHI in growing season (Huang et al., 2017). Although the urban-rural difference of surface heat storage also increased in the growing season, the decreased nighttime SUHI indicated the dominant role of the urbanrural difference in the thermal inertia, instead of the urban-rural difference in the surface heat storage, on the seasonal variation of SUHI.

The positive correlations between the ATC model parameters and ISA in Fig. 4 indicated that the interannual variation of SUHI was mainly controlled by the increased ISA. The $\Delta_{\text{u-r}}\text{DTR}$'s increasing trends in summer and decreasing trends in winter indicated that increased ISA decreased surface thermal inertia in winter and increased thermal inertia in summer in the newly urbanized areas. Meanwhile, the increased ISA could decrease evapotranspiration. The decreased thermal inertia in winter led to more negative daytime SUHI and the increase in nighttime SUHI (Fig. 6). Meanwhile, in summer, the increased thermal inertia and decreased evapotranspiration led to an increase in daytime SUHI. However, the increased thermal inertia did not lead to a decrease in nighttime SUHI. This may be because the urbanized impervious surface also increased heat storage, which could offset the negative impact of increased thermal inertia on nighttime SUHI.

We also found that the summer daytime SUHI in the central areas did not increase with urbanization, but showed decreasing trends in all three cities in spite of the slow increase in ISA in these buffers, opposite to the trends of SUHI in other buffers (Fig. 6). The interannual change of vegetation could be the main underlying factor, which has been reported by previous study (Gui et al., 2019). Vegetation in cities could decrease SUHI by increasing evapotranspiration. We found that the daytime S_M showed a positive correlation with the urban-rural difference of EVI (Fig. 8). During the study period, the EVI in the urban center generally showed increasing trends, while that in the rural area showed slightly decreasing trends, resulting in the decreasing ruralurban difference of EVI (Fig. 9). The decreasing difference in vegetation between the central and rural buffers reduced the difference of evapotranspiration between them, leading to the decreased SUHI in the central buffer. Moreover, although both ISA and EVI increased in the central buffer, the decreased SUHI indicated that the impact of increased vegetation exceeded the impact of increased ISA on daytime SUHI in the summer. This implies that planting trees is an efficient way to mitigate the daytime SUHI.

5. Conclusions

This study developed a framework to investigate the response of SUHI to urban expansion in the JJJ region using the ATC model. We generated the annual SUHI cycle at the buffer level from 2003 to 2018 over 13 major citis in the JJJ region and evaluated its accuracy. Then we investigated the relationship between ATC model parameters and ISA and the spatiotemporal dynamic of SUHI. Finally, we examined the underlying mechanism through the comparisons of the interannual variations of DTR and EVI across urban and rural gradients.

Results showed the derived SUHI from the ATC model generally matched the observations. The model parameters (S_M and S_A) showed significant urban-rural differences and positive correlations with ISA spatially, indicating the mean and amplitude of annual SUHI cycle increased with urban expansion. The spatiotemporal patterns of SUHI

showed different interannual dynamic across seasons and the time of the day and over urban-rural gradients. The daytime SUHI was negative in winter with decreasing interannual trends, but was positive in summer with increasing interannual trends. The nighttime SUHI was always positive with the largest values in winter and showed slightly increasing interannual trends. Spatially, the interannual variation of SUHI mainly occurred in the suburban buffers where showing the largest increase in the ISA. Temporally, daytime SUHI was more sensitive to urban expansion than nighttime SUHI. The seasonal variation of SUHI was mainly controlled by vegetation covering in rural areas through changing the thermal inertia and evapotranspiration, while the interannual variation of SUHI was mainly controlled by urban expansion. In addition, urban greening in the city center could lead to the decrease in daytime SHUI in summer.

Our study presented the variations of SUHI across spatial (e.g. urban center and suburban areas) and temporal (i.e., annual, seasonal, and diurnal) scales and the underlying mechanism under urbanization. We found that the fast urbanization was one of the most important driving forces of the intensification in the SUHI. Future urbanization could further strengthen SUHI and increase the heat risk in this region. Besides, we found the positive effect of urban greening in mitigating SUIH in summer. All these findings deepened our understanding of the response of SUHI to urbanization and provided a scientific basis for the prediction and mitigation of future heat risk for urban sustainability. This study validated the reliability of the ATC model in studying SUHI's variation. The relationships between the ATC model parameters and ISA can be potentially used for predicting future SUHI.

Meanwhile, it is worth to note that the validity of the ATC model is dependent on the assumption that the evolution of surface temperature within an annual cycle is mainly driven by the solar declination (Bechtel, 2012). The derived SUHI represents the climatology of annual SUHI on an annual time scale. However, the real annual temperature and SUHI cycle are complicated and also affected by several short-term factors, such as the changes in the weather, snow/ice cover, vegetation phenology, irrigation, and soil moisture dynamics (Huang et al., 2016). Future studies can further explore SUHI using the ATC model with the consideration of these factors. Additionally, the mismatch in the time series of SUHI and ISA due to the data availability may lead to uncertainties in the analysis of SUHI dynamic after 2015. Nevertheless, given the continuous urbanization in the study areas and the consistent interannual trend of the SUHI before and after 2015, the caused uncertainties in the conclusions should be rather minor.

Declaration of competing interest

The authors declare that they have no known competing financial interests or personal relationships that could have appeared to influence the work reported in this paper.

Acknowledgments

This study was supported by the National Science Foundation (CBET-1803920).

Appendix A. Supplementary data

Supplementary data to this article can be found online at https://doi.org/10.1016/j.gsf.2021.101141.

References

Alberti, M., Correa, C., Marzluff, J.M., Hendry, A.P., Palkovacs, E.P., Gotanda, K.M., Hunt, V.M., Apgar, T.M., Zhou, Y., 2017. Global urban signatures of phenotypic change in animal and plant populations. Proceed. Nation. Acad. Sci. U.S.A. 114, 8951–8956.

Bechtel, B., 2012. Robustness of annual cycle parameters to characterize the urban thermal landscapes. IEEE Geosci. Remote Sens. Lett. 9, 876–880.

ARTICLE IN PRESS

H. Li, Y. Zhou, G. Jia et al. Geoscience Frontiers xxx (2021) xxx

- Bechtel, B., 2015. A new global climatology of annual land surface temperature. Remote Sens. 7, 2850–2870.
- Bechtel, B., Demuzere, M., Mills, G., Zhan, W., Sismanidis, P., Small, C., Voogt, J., 2019. SUHI analysis using local climate zones—a comparison of 50 cities. Urban Clim. 28, 100451.
- Carnahan, W.H., Larson, R.C., 1990. An analysis of an urban heat sink. Remote Sens. Environ. 33 (1), 65–71.
- Chakraborty, T., Lee, X., 2019. A simplified urban-extent algorithm to characterize surface urban heat islands on a global scale and examine vegetation control on their spatiotemporal variability. Int. J. Appl. Earth Obs. Geoinf. 74, 269–280.
- Christen, A., Vogt, R., 2004. Energy and radiation balance of a central European city. Int. J. Climatol. 24 (11), 1395–1421.
- Connors, J.P., Galletti, C.S., Chow, W.T., 2013. Landscape configuration and urban heat island effects: assessing the relationship between landscape characteristics and land surface temperature in Phoenix. Arizona. Landsc. Ecol. 28 (2), 271–283.
- Constantinescu, D., Cheval, S., Caracaş, G., Dumitrescu, A., 2016. Effective monitoring and warning of Urban Heat Island effect on the indoor thermal risk in Bucharest (Romania). Energy Build. 127, 452–468.
- Guhathakurta, S., Gober, P., 2007. The impact of the Phoenix urban heat island on residential water use. J. Am. Plan. Assoc. 73 (3), 317–329.
- Gui, X., Wang, L., Yao, R., Yu, D., 2019. Investigating the urbanization process and its impact on vegetation change and urban heat island in Wuhan, China. Environ. Sci. Pollut. Res. 26 (30), 30808–30825.
- Hu, L., Brunsell, N.A., 2013. The impact of temporal aggregation of land surface temperature data for surface urban heat island (SUHI) monitoring. Remote Sens. Environ. 134, 162–174.
- Hu, L., Brunsell, N.A., 2015. A new perspective to assess the urban heat island through remotely sensed atmospheric profiles. Remote Sens. Environ. 158, 393–406.
- Huang, F., Zhan, W., Voogt, J., Hu, L., Wang, Z., Quan, J., Ju, W., Guo, Z., 2016. Temporal upscaling of surface urban heat island by incorporating an annual temperature cycle model: a tale of two cities. Remote Sens. Environ. 186, 1–12.
- Huang, F., Zhan, W., Wang, Z., Wang, K., Chen, J.M., Liu, Y., Lai, J., Ju, W., 2017. Positive or negative? Urbanization-induced variations in diurnal skin-surface temperature range detected using satellite data. J. Geophys. Res.-Atmos. 122 (24), 13–229.
- Li, H., Wang, A., Yuan, F., Guan, D., Jin, C., Wu, J., Zhao, T., 2016. Evapotranspiration dynamics over a temperate meadow ecosystem in eastern Inner Mongolia, China. Environ. Earth Sci. 75 (11), 978. https://doi.org/10.1007/s12665-016-5786-z.
- Li, D., Liao, W., Rigden, A.J., Liu, X., Wang, D., Malyshev, S., Shevliakova, E., 2019a. Urban heat island: aerodynamics or imperviousness? Sci. Adv. 5 (4), eaau4299.
- Li, H., Meier, F., Lee, X., Chakraborty, T., Liu, J., Schaap, M., Sodoudi, S., 2018a. Interaction between urban heat island and urban pollution island in Berlin during summer. Sci. Total Environ. 636. 818–828.
- Li, H., Zhou, Y., Li, X., Meng, L., Wang, X., Wu, S., Sodoudi, S., 2018b. A new method to quantify surface urban heat island intensity. Sci. Total Environ. 624, 262–272.
- Li, H., Wolter, M., Wang, X., Sodoudi, S., 2018d. Impact of land cover data on the simulation of urban heat island for Berlin using WRF coupled with bulk approach of Noah-LSM. Theor. Appl. Climatol. 34, 67–81.
- Li, H., Sodoudi, S., Liu, J., Tao, W., 2020. Temporal variation of urban aerosol pollution island and its relationship with urban heat island. Atmos. Res. 241, 104957. https://doi.org/10.1016/j.atmosres.2020.104957.
- Li, X., Zhou, Y., Asrar, G.R., Mao, J., Li, X., Li, W., 2017a. Response of vegetation phenology to urbanization in the conterminous United States. Glob. Chang. Biol. 23, 2818–2830.
- Li, X., Zhou, Y., Asrar, G.R., Imhoff, M., Li, X., 2017b. The surface urban heat island response to urban expansion: a panel analysis for the conterminous United States. Sci. Total Environ. 605, 426–435.
- Li, X., Zhou, Y., Asrar, G.R., Zhu, Z., 2018c. Creating a seamless 1 km resolution daily land surface temperature dataset for urban and surrounding areas in the conterminous United States. Remote Sens. Environ. 206, 84–97.
- Li, X., Zhou, Y., Zhu, Z., Liang, L., Yu, B., Cao, W., 2018e. Mapping annual urban dynamics (1985–2015) using time series of Landsat data. Remote Sens. Environ. 216, 674–683.

- Li, X., Zhou, Y., Yu, S., Jia, G., Li, H., Li, W., 2019c. Urban heat island impacts on building energy consumption: a review of approaches and findings. Energy 174 (1), 407–419.
- Liu, X., Zhou, Y., Yue, W., Li, X., Liu, Y., Lu, D., 2020. Spatiotemporal patterns of summer urban heat island in Beijing, China using an improved land surface temperature. J. Clean. Prod. 257, 120529.
- Meng, L., Mao, J., Zhou, Y., Richardson, A.D., Lee, X., Thornton, P.E., Ricciuto, D.M., Li, X., Dai, Y., Shi, X., Jia, G., 2020. Urban warming advances spring phenology but reduces the response of phenology to temperature in the conterminous United States. Proceed. Nation. Acad. Sci. U.S.A. 117 (8), 4228–4233. https://doi.org/10.1073/pnas.1911117117.
- Oke, T.R., 1982. The energetic basis of the urban heat island. Q. J. R. Meteorol. Soc. 108 (455), 1–24.
- Peng, S., Piao, S., Ciais, P., Friedlingstein, P., Ottle, C., Bréon, F.M., Nan, H., Zhou, L., Myneni, R.B., 2012. Surface urban heat island across 419 global big cities. Environ. Sci. Technol. 46 (2), 696–703.
- Tang, J., Di, L., Xiao, J., Lu, D., Zhou, Y., 2017. Impacts of land use and socioeconomic patterns on urban heat Island. Int. J. Remote Sens. 38 (11), 3445–3465.
- Varquez, A.C., Kanda, M., 2018. Global urban climatology: a meta-analysis of air temperature trends (1960–2009). NPJ Clim. Atmos. Sci. 1 (1), 32.
- Wan, Z., 2014. New refinements and validation of the collection-6 MODIS land-surface temperature/emissivity product. Remote Sens. Environ. 140, 36–45.
- Wang, K., Wang, J., Wang, P., Sparrow, M., Yang, J., Chen, H., 2007. Influences of urbanization on surface characteristics as derived from the Moderate-Resolution Imaging Spectroradiometer: A case study for the Beijing metropolitan area. J. Geophys. Res.-Atmos. 112, D22S06. https://doi.org/10.1029/2006JD007997.
- Wang, Y., Wang, A., Zhai, J., Tao, H., Jiang, T., Su, B., Yang, J., Wang, G., Liu, Q., Gao, C., Kundzewicz, Z.W., 2019. Tens of thousands additional deaths annually in cities of China between 1.5 °C and 2.0 °C warming. Nat. Commun. 10, 3376. https://doi.org/10.1038/s41467-019-11283-w.
- Weng, Q., Fu, P., 2014. Modeling annual parameters of clear-sky land surface temperature variations and evaluating the impact of cloud cover using time series of Landsat TIR data. Remote Sens. Environ. 140, 267–278.
- Wu, J., 2014. Urban ecology and sustainability: the state-of-the-science and future directions, Landsc. Urban Plan. 125, 209–221.
- Yao, R., Wang, L., Huang, X., Gong, W., Xia, X., 2019. Greening in rural areas increases the surface urban heat island intensity. Geophys. Res. Lett. 46 (4), 2204–2212.
- Yue, W., Liu, X., Zhou, Y., Liu, Y., 2019. Impacts of urban configuration on urban heat island: an empirical study in China mega-cities. Sci. Total Environ. 671, 1036–1046.
- Zhao, G., Dong, J., Cui, Y., Liu, J., Zhai, J., He, T., Zhou, Y., Xiao, X., 2019. Evapotranspiration-dominated biogeophysical warming effect of urbanization in the Beijing-Tianjin-Hebei region, China. Clim. Dyn. 52, 1231–1245.
- Zhou, B., Rybski, D., Kropp, J.P., 2017. The role of city size and urban form in the surface urban heat island. Sci. Rep. 7 (1), 4791.
- Zhou, D., Zhao, S., Zhang, L., Sun, G., Liu, Y., 2015b. The footprint of urban heat island effect in China. Sci. Rep. 5, 11160.
- Zhou, D., Xiao, J., Bonafoni, S., Berger, C., Deilami, K., Zhou, Y., Frolking, S., Yao, R., Qiao, Z., Sobrino, J., 2019. Satellite remote sensing of surface urban heat islands: progress, challenges, and perspectives. Remote Sens. 11 (1), 48.
- Zhou, Y., Smith, S.J., Elvidge, C.D., Zhao, K., Thomson, A., Imhoff, M., 2014. A cluster-based method to map urban area from DMSP/OLS nightlights. Remote Sens. Environ. 147, 173, 185
- Zhou, Y., Smith, S.J., Zhao, K., Imhoff, M., Thomson, A., Bond-Lamberty, B., Asrar, G.R., Zhang, X., He, C., Elvidge, C.D., 2015a. A global map of urban extent from nightlights. Environ. Res. Lett. 10, 054011.
- Zhou, Y., Li, X., Asrar, G.R., Smith, S.J., Imhoff, M., 2018. A global record of annual urban dynamics (1992–2013) from nighttime lights. Remote Sens. Environ. 219, 206–220.
- Zou, Z., Zhan, W., Liu, Z., Bechtel, B., Gao, L., Hong, F., Huang, F., Lai, J., 2018. Enhanced modeling of annual temperature cycles with temporally discrete remotely sensed thermal observations. Remote Sens. 10 (4), 650.